Data assimilation of turbulent separated flows using single synthetic and experimental wall-pressure data

Cynthia Tayeh, Vincent Mons, Olivier Marquet

Data assimilation of turbulent separated flows using single synthetic and experimental wall-pressure data

C. Tayeh[1], V. Mons[1] † and O. Marquet[1]

[1]DAAA, ONERA, Université Paris Saclay, F-92190 Meudon, France

(Received xx; revised xx; accepted xx)

This paper investigates the reconstruction of turbulent mean flows around an airfoil near stalling conditions based on numerical or experimental wall observations at a very few (one or two) locations on the suction and pressure sides of the airfoil. The reconstruction procedure consists in using the considered wall data to determine a correction to the Reynolds-Averaged Navier-Stokes (RANS) equations through a variational data assimilation technique. Mean-flow fields obtained from Direct Numerical Simulations (DNS) around a NACA4412 airfoil at chord-based Reynolds number $Re_c = 3.5 \cdot 10^5$ and various angles of attack (8°, 10° and 11°) are first used both to generate synthetic observations and to assess the quality of the full mean flows that are recovered through data assimilation. While the assimilation of wall skin-friction observations leads to poor reconstructions, relying on wall-pressure data at a single location allows to recover the turbulent flow separation at the trailing edge that is not captured by the baseline RANS model. A remarkable accuracy is achieved for most observation locations, on both suction and pressure sides of the airfoil. At locations where the pressure predicted by the baseline model is similar to the pressure data, the flow reconstruction is poor. The addition of a second wall-pressure observation then allows to retrieve a mean flow whose quality is similar to that in successful single-data cases, suggesting that multiple wall-pressure sensors are of interest for robustness rather than accuracy of the flow reconstruction. Finally, it is shown that the turbulent flow separation can also be successfully recovered through the assimilation of a single experimental wall-pressure measurement.

Key words:

MSC Codes *(Optional)* Please enter your MSC Codes here

1. Introduction

The characterization of complex turbulent flows as encountered in many industrial applications often relies on both numerical simulations and experiments. For flows at high Reynolds numbers, the computational cost of Direct Numerical Simulations (DNS) is still nowadays too prohibitive. Simulation of the Reynolds-Averaged Navier-Stokes (RANS) equations, which

† Email address for correspondence: vincent.mons@onera.fr

solve for the mean flow only and model the full turbulent spectrum, is therefore a popular numerical approach in the industry. Nevertheless, deficiencies in turbulence modelling may significantly alter the fidelity of such simulations, in particular for massively separated flows. On the other hand, wind-tunnel experiments on reduced-scale models combined with advanced measurements techniques may provide valuable information about flows of interest. The on-going development of non-intrusive optical techniques may indeed give detailed insight into planar or three-dimensional velocity fields and their statistics. However, the difficulty in implementing these techniques prevents from performing such measurements in complex flow configurations. More often, reduced-scale models are equipped with static pressure probes, yielding only wall-pressure measurements at a few locations. The objective of the present paper is to use such sparse wall measurements to infer accurate full mean flows based on RANS modelling.

In the past decade, data assimilation methods as originally developed in meteorology and oceanography have been used to rigorously merge experimental results with RANS simulations in order to overcome their respective limitations (Xiao & Cinnella 2019). Among the various data assimilation studies using mean-velocity observations, Symon *et al.* (2017) investigated the reconstruction of the mean flow around an idealized airfoil from time-averaged two-dimensional Particle Image Velocimetry (PIV) data, while the use of pointwise observations was studied in Franceschini *et al.* (2020); Mons & Marquet (2021). Fewer studies have focused on flow reconstruction based on wall data only, still restricting the following discussion to RANS-based data assimilation, while it may be mentioned that DNS has also been considered for such a task (Buchta *et al.* 2022). Kato *et al.* (2015); Singh & Duraisamy (2016); Belligoli *et al.* (2019) relied on the pressure distribution at the surface of various airfoils to reconstruct subsonic and transonic flows around two-dimensional airfoils and three-dimensional wings (Kato *et al.* 2015). Interestingly, good convergence of the data assimilation procedure was obtained by Belligoli *et al.* (2019) using only five pressure observations, but the quality of the reconstructed mean flows was barely assessed on a quantitative level. Li *et al.* (2022) considered synthetic wall-pressure distributions to successfully estimate various turbulent flow configurations. Ben Ali *et al.* (2022) reconstructed the three-dimensional mean-flow around a high-rising building from experimental wall-pressure measurements. Inspired by the encouraging results obtained in these studies, we here further investigate the capability of data assimilation based on wall quantities to accurately estimate turbulent separated flows around a NACA4412 airfoil at $Re_c = 3.5 \cdot 10^5$. Unlike previous studies that relied on a significant number of data, we will here focus on the consideration of extremely scarce wall data, i.e. that are available at a single or two locations on the airfoil. Moreover, before considering experimental data, synthetic numerical results will first be employed to enable a rigorous assessment of the capability of the present data assimilation approach to accurately reconstruct full mean-velocity fields.

The paper is organized as follows. The flow configuration, along with the reference DNS and experimental results, RANS model and data assimilation approach for mean-flow reconstruction are introduced in §2. Data assimilation results are described in §3. Concluding remarks and perspectives are drawn in §4.

2. Flow configuration and data assimilation methodology

2.1. *DNS and experimental results*

Direct Numerical Simulations (DNS) of the flow past a NACA4412 profile were recently performed by Gleize *et al.* (2022) to provide a detailed database of trailing-edge separated flows near stall. These simulations were carried out for a wing chord-based Reynolds number

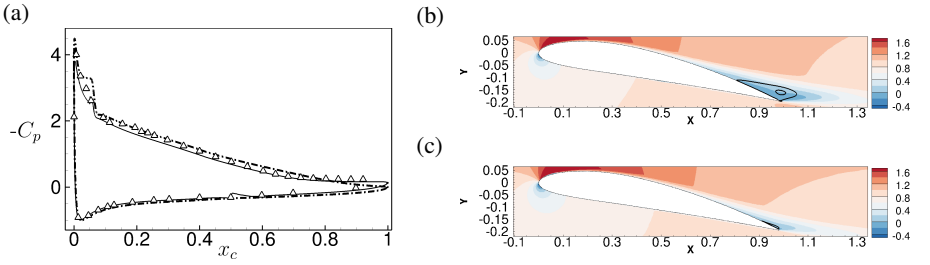

Figure 1: (a) Pressure coefficient C_p for experimental (triangles), DNS (solid line), and baseline RANS results (dash-dotted line) at $\alpha = 11^\circ$. (b,c) Streamwise mean velocity at the same incidence obtained with (b) DNS or (c) baseline RANS. A few streamlines are reported in full lines to emphasize the recirculation region.

of $Re_c = 3.5 \cdot 10^5$ and an infinite upstream Mach number of 0.117, corresponding to an almost incompressible flow regime. In the following, all quantities are normalized by the chord of the airfoil and the uniform free-stream velocity. Various angles of incidences between the streamwise and chordwise directions, denoted by α, were considered in the pre-stall regime (8°, 10°, 11°). Particular attention was devoted to triggering the laminar-turbulent transition without significantly disturbing the flow. This was achieved through adding small cylindrical roughness elements on suction and pressure sides of the wing, which are equidistantly distributed in the spanwise direction. These roughness elements are located at chordwise coordinates $x_c = 0.05$ and $x_c = 0.5$ on suction and pressure sides, respectively. The mean flow field that is obtained through spanwise and time average of DNS results for the incidence $\alpha = 11^\circ$ is illustrated in figure 1(b), the corresponding wall-pressure coefficient C_p being reported in figure 1(a). Noteworthy flow features at this incidence are the turbulent separation and significant recirculation region close to the trailing edge.

Wind-tunnel experiments were performed on the same airfoil in a subsonic wind tunnel for similar inflow conditions and positions of triggered laminar-turbulent transition. Static pressure measurements are available at mid-span of the wing for various locations on the pressure and suction sides of the airfoil, as reported with triangles in figure 1(a). Note that the experimental and DNS data appear in good agreement over most of the wing profile, discrepancies being mainly observed from the leading edge to $x_c = 0.4$ on the suction side. The goal of the following data assimilation methodology is to reconstruct full mean flows based on such either DNS or experimental wall data.

2.2. *Baseline RANS results and data assimilation procedure*

As a much cheaper alternative to the above DNS, one could consider the use of Reynolds-Averaged Navier-Stokes (RANS) models to directly estimate the present mean flows of interest. We here rely on the Spalart-Allmaras model (Spalart & Allmaras 1994), which has been mainly developed for aerodynamic applications. This model relies on the Boussinesq hypothesis to close the here two-dimensional incompressible RANS equations for the mean-flow velocity $\tilde{\mathbf{u}}$ and pressure fields where the total viscosity is the sum of the molecular viscosity ($\nu = 1/Re$) and eddy-viscosity $\tilde{\nu}_t$ field. In the Spalart-Allmaras model, $\tilde{\nu}_t$ is deduced from an eddy-viscosity-like variable $\tilde{\nu}$ for which is prescribed a governing equation, as specified below. The RANS equations are here solved and discretized with a finite-element method as implemented in the software FreeFEM (Hecht 2012) using second-order Taylor-Hood elements. Streamline-Upwind Petrov-Galerkin and Grad-Div stabilizations are implemented to tackle the present convection-dominated flows. The extent of the computational domain corresponds to that used in the above DNS (Gleize *et al.* 2022).

The mesh is composed of $1.4 \cdot 10^5$ anisotropic triangles whose distribution is obtained by an automatic adaptation procedure based on the Hessian of the velocity, pressure and eddy-viscosity fields. More details are available in Franceschini *et al.* (2020). Results obtained with this numerical approach are illustrated in figure 1(a,c) for $\alpha = 11°$. Large discrepancies between RANS and DNS mean-velocity fields are identified close to the trailing edge as RANS fails to correctly capture the recirculation region. To a lesser extent, differences also exist between wall-pressure coefficients of RANS and DNS (or experimental) results. To enhance the RANS capability to predict such a separated turbulent flow, we here investigate a data assimilation approach based on limited wall data extracted from DNS or experiments which are used to correct the RANS equations. In the case of limited observations, Franceschini *et al.* (2020) showed that better reconstruction results were obtained when adjusting the turbulence model compared to acting in the momentum equations. Therefore, a corrective spatially-dependent field $\tilde{g}$ is introduced in the Spalart-Allmaras equation which governs the eddy-viscosity-like variable $\tilde{\nu}$ according to

$$\tilde{\mathbf{u}} \cdot \nabla\tilde{\nu} - \nabla \cdot (\eta(\tilde{\nu})\nabla\tilde{\nu}) - s(\tilde{\nu}, \nabla\tilde{\nu}, \nabla\tilde{\mathbf{u}}) = \tilde{g}\tilde{\nu}, \tag{2.1}$$

where $\eta(\tilde{\nu})$ is a diffusion coefficient, and $s(\tilde{\nu}, \nabla\tilde{\nu}, \nabla\tilde{\mathbf{u}})$ gathers production, destruction and cross-diffusion terms (Spalart & Allmaras 1994). Baseline RANS results correspond to $\tilde{g} = 0$. Note that the corrective field $\tilde{g}$ is here premultiplied by $\tilde{\nu}$ in (2.1) so as to naturally restrict model corrections to regions with non-negligible turbulence intensity, i.e. where $\tilde{\nu} \neq 0$, and to favor them in regions with high turbulence levels. Other model corrections have been proposed in previous studies (Singh & Duraisamy 2016; Franceschini *et al.* 2020) and we refer to Cato *et al.* (2023) for a detailed assessment of these various approaches. Among them, the best results were still obtained with the multiplicative correction $\tilde{g}$ for the present flow configuration. This correction is determined so as to minimize the discrepancies between data $\bar{\mathbf{m}}$ and the estimation of the same quantity through the RANS model, denoted by $\tilde{\mathbf{m}}(\tilde{g})$. In a least-square variational data assimilation approach, we thus aim to identify the field $\tilde{g}$ that minimizes the following cost function

$$\mathcal{J}(\tilde{g}) = \|\bar{\mathbf{m}} - \tilde{\mathbf{m}}(\tilde{g})\|^2_{\mathcal{M}}, \tag{2.2}$$

where $\|\cdot\|_{\mathcal{M}}$ corresponds to the norm that is associated to the observation space. In the following, the data $\bar{\mathbf{m}}$ will mainly correspond to a wall quantity such as the pressure coefficient C_p at a single location on the airfoil. In this case, $\|\cdot\|_{\mathcal{M}}$ will simply correspond to the Euclidean norm for $\mathbb{R}$. The minimization of $\mathcal{J}$ with respect to the model correction is performed through an iterative gradient-based descent method. The gradient of $\mathcal{J}$ with respect to $\tilde{g}$ that is required by such a procedure is obtained following the adjoint approach to take into account the equality constraint that is formed by the RANS equations. The first-guess of the optimization procedure corresponds to baseline RANS (i.e. $\tilde{g} = 0$). More details about the present variational data assimilation methodology may be found in Franceschini *et al.* (2020). Contrary to previous studies (Ben Ali *et al.* 2022), one may emphasize the fact that we do not here rely on any sort of regularization, such as penalization or gradient smoothing, in the data assimilation procedure.

3. Results

The present data assimilation methodology is first applied to the reconstruction of the above-discussed mean flow at $\alpha = 11°$. Before considering experimental observations, synthetic observations extracted from DNS are used to enable a quantitative assessment of the reconstructions, which will be the main focus in the following. We first show results using single wall data as observation in the data assimilation procedure and compare them

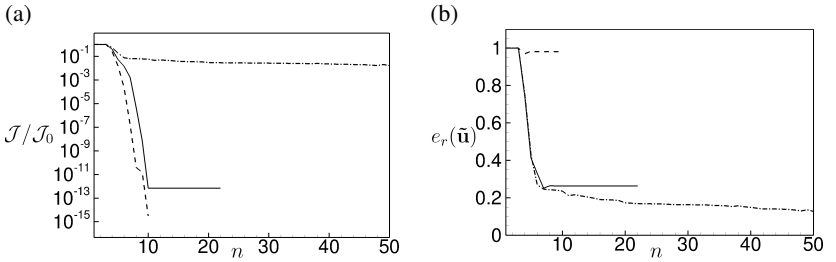

Figure 2: Evolution along the iteration n of the data assimilation procedure of (a) the normalized cost function $\mathcal{J}/\mathcal{J}_0$ and (b) reconstruction error $e_r(\tilde{\mathbf{u}})$ when the considered observation is C_p at $x_c = 0.4$ on the suction side (solid line), C_f at the same location (dashed line) or the full DNS mean-velocity field (dash-dotted line).

to reference results obtained with the full DNS mean-velocity field $\bar{\mathbf{u}}_d$ as observation, i.e. $\bar{\mathbf{m}} = \bar{\mathbf{u}}_d$. For single wall data, the observation vector $\bar{\mathbf{m}}$ reduces to a scalar quantity that is either the wall-pressure C_p or the wall skin-friction C_f coefficient at the chordwise position $x_c = 0.4$ on the suction side of the airfoil. The convergence of the data assimilation procedure for these different types of observations is first illustrated in figure 2(a), which reports the evolution of the cost function $\mathcal{J}$ along the optimization iteration, normalized by its initial value $\mathcal{J}_0$. When using single wall data (solid and dashed lines), the cost functions decrease by several order of magnitude in around 10 iterations. On the other hand, when considering the full mean-velocity field (dash-dotted line), more than 100 iterations are necessary to decrease the cost function by only 2 orders of magnitude. This improved convergence of the algorithm in the former cases implies a reduced computational cost, that here amounts to performing less than 10 RANS and adjoint computations, but is of interest only if the reconstructed mean flow compares well with the reference DNS results. To assess such reconstruction capability, figure 2(b) depicts the evolution of the relative error $e_r(\tilde{\mathbf{u}})$ in the estimation of the mean-velocity field, which is defined as

$$e_r(\tilde{\mathbf{u}}) = \frac{e(\tilde{\mathbf{u}})}{e(\tilde{\mathbf{u}}_b)}, \qquad e(\tilde{\mathbf{u}}) = \sqrt{\frac{\int_{\Omega_m} ((\bar{\mathbf{u}}_d - \tilde{\mathbf{u}}) \cdot (\bar{\mathbf{u}}_d - \tilde{\mathbf{u}}))\, d\Omega_m}{\int_{\Omega_m} (\bar{\mathbf{u}}_d \cdot \bar{\mathbf{u}}_d)\, d\Omega_m}}, \tag{3.1}$$

where $\bar{\mathbf{u}}_d$ and $\tilde{\mathbf{u}}_b$ refer to DNS and baseline RANS mean-velocity fields, respectively. The sub-domain Ω_m is centered around the airfoil according to $\Omega_m = \{\mathbf{x} = (x, y);\ -0.5 < x < 1.5, -0.3 < y < 0.2\}$. The error $e_r(\tilde{\mathbf{u}})$ directly quantifies the enhancement in the estimation of the velocity field compared to baseline RANS, which corresponds to $e_r(\tilde{\mathbf{u}}_b) = 1$. The use of the single skin-friction coefficient data (dashed line) leads to very limited improvement in the reconstruction since $e_r(\tilde{\mathbf{u}}) = 0.980$ at the end of the optimization. In contrast, the use of the single pressure coefficient enables a remarkable decrease in the reconstruction error (solid line), converging towards $e_r(\tilde{\mathbf{u}}) = 0.264$. Interestingly, this error is very similar to that obtained after $\sim$ 10 iterations when using the full mean-velocity field as observation (dash-dotted line). In this latter case, a slow improvement of the reconstruction error is then observed since more than 90 supplementary iterations are necessary to divide the error by three ($e_r(\tilde{\mathbf{u}}) = 0.081$ at the final iteration).

Figures 3(a,c) show the streamwise velocity of the mean flows that are reconstructed based on the single C_p and C_f data, respectively. In the latter case, the reconstructed flow is almost unchanged compared to the baseline RANS solution (figure 1c). On the other hand, the mean flow reconstructed with the single wall-pressure data exhibits a separation of the turbulent boundary layer leading to a recirculation region close to the trailing edge, as observed in the

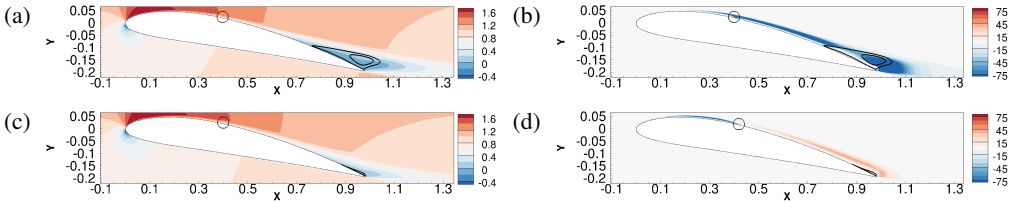

Figure 3: (a,c) Streamwise mean velocity and (b,d) corrective field $\tilde{g}\tilde{\nu}/\nu$ at the last iteration of the data assimilation procedure with a single observation of (a,b) C_p or (c,d) C_f at position $x_c = 0.4$ on the suction side of the airfoil, shown with black circles.

DNS results (figure 1b), thus entailing low velocity error $e_r(\tilde{\mathbf{u}})$. This improvement in the estimation of the mean velocity is also associated to better predicted aerodynamic coefficients. Notably, the reconstructed lift coefficient $C_L = 1.255$ compares very well with that computed with DNS ($C_L = 1.259$), unlike that obtained with baseline RANS ($C_L = 1.457$). To better understand the differences between the reconstruction performances obtained with single C_p and C_f data, the turbulent-model corrections at the final iteration of the data assimilation procedure are shown in figures 3(b,d), respectively. The quantity $\tilde{g}\tilde{\nu}$ is displayed as it is the effective forcing in the turbulence model (2.1), normalized by the kinematic viscosity ν. In both cases, the correction is distributed over a large part of the suction side, despite the local nature of the observation. The correction obtained with the wall-pressure data (figure 3b) is overall negative and therefore contributes to decrease the eddy-viscosity. This eddy-viscosity destruction is sufficiently large in the turbulent boundary layer to induce its separation around $x_c = 0.79$, while the largest magnitude of the correction is reached further downstream in the rear part of the recirculation region. The correction obtained with the wall skin-friction observation (figure 3d) is of much smaller magnitude. Moreover, being positive downstream of the observation, it increases the production of eddy-viscosity, thus explaining the inability of data assimilation to recover significant flow separation in this case (figure 3c).

As a first step towards investigating the influence of the observation location on mean-flow reconstruction, figure 4 shows results obtained with single wall-pressure or skin-friction data at location $x_c = 0.2$ on the pressure side. Strikingly, the velocity and corrective fields obtained with the present wall-pressure data (figures 4a,b) are very similar to those obtained with the previous pressure observation on the suction side (figure 3a,b). Clearly, despite the facts that the pressure observation is located at the pressure side and that discrepancies between baseline RANS and DNS are weaker there compared to the suction side, the data assimilation procedure has still identified a model correction that is spatially-distributed over the suction side. It is noteworthy that such a distribution of the corrective field is obtained for most of the observation positions that are investigated in the following and for which low reconstruction error is achieved ($e_r(\tilde{\mathbf{u}}) < 0.3$). Turning now to results obtained with the wall skin-friction observation on the pressure side, the corrective field is also located on the suction side (figure 4d). Being negative unlike that obtained with the observation on the suction side (figure 3d), it here contributes to decrease the eddy-viscosity. However, its magnitude is too small to sufficiently favor an earlier separation of the turbulent boundary layer and to increase the size of the recirculation region (figure 4c).

Given the capability of wall-pressure-based data assimilation in accurately reconstructing the reference mean flow, we will only focus on this type of observation in the following and assess the robustness of the above results with respect to various factors. The influence of the location of the single C_p observation is now systematically investigated. Figures 5(a,b) report the reconstruction error $e_r(\tilde{\mathbf{u}})$ at the end of the data assimilation procedure for various positions on the suction and pressure sides, respectively. The low level of reconstruction

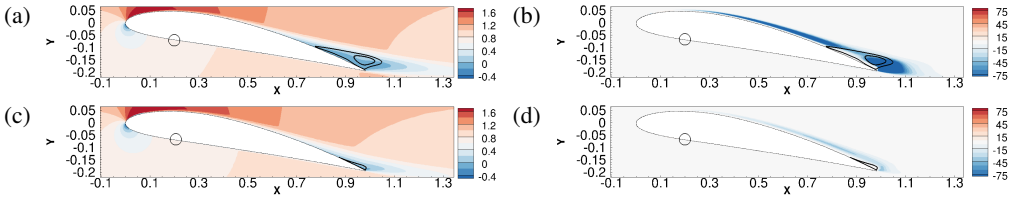

Figure 4: Same legend as figure 3 but for a single observation at $x_c = 0.2$ on the pressure side of the airfoil.

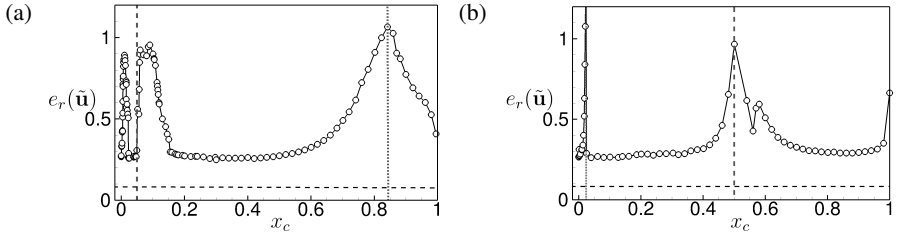

Figure 5: Reconstruction error $e_r(\tilde{\mathbf{u}})$ at the end of the data assimilation procedure versus the location of the single C_p observation on (a) the suction side or (b) the pressure side. The vertical dashed lines report the locations of the laminar-turbulent transition zones. The vertical dotted lines correspond to the locations where baseline RANS predicts the same value of C_p as in DNS. For the sake of comparison, the horizontal dashed lines report the value of $e_r(\tilde{\mathbf{u}})$ when the full DNS mean-velocity field is observed.

error ($e_r(\tilde{\mathbf{u}}) < 0.3$) that was achieved for $x_c = 0.4$ on the suction side or $x_c = 0.2$ on the pressure side is reached for most of the investigated locations. This confirms the impressive capability of data assimilation in reconstructing the whole flow based on a single C_p data. There are however some observation positions for which data assimilation is unsuccessful in improving RANS results. These locations cluster around two types of positions that are shown with vertical dashed and dotted lines in the figure: positions where the laminar-turbulent transition is triggered in the boundary layer (dashed lines) and positions where the value of C_p predicted by baseline RANS is already equal to the reference one (dotted lines). The poor reconstruction performances for observations close to the laminar-turbulent transition points may be attributed to the particular way transition was imposed in the present DNS results, as detailed in §2.1. On the other hand, if baseline RANS and reference C_p values are already close, the cost function $\mathcal{J}$ is almost 0 from the start so that the data assimilation procedure can not really operate.

To avoid the latter situation and thus improve the robustness of the mean-flow reconstruction, we now investigate the use of a second wall-pressure observation in the data assimilation procedure. Focusing on two observations located on the suction side of the airfoil and excluding positions close to the transition region ($x_c < 0.2$), figure 6 reports the reconstruction error $e_r(\tilde{\mathbf{u}})$ obtained when one of the observation location $x_{c(1)}$ is varied, while the second one $x_{c(2)}$ is kept fixed. Through figure 6(a), we first consider the fixed position $x_{c(2)} = 0.4$ which corresponds to an already successful reconstruction in the single-data case as illustrated above. It appears that all observation pairs including the one at $x_{c(2)} = 0.4$ provide satisfactory reconstruction results, while the latter are not substantially improved compared to only considering the observation at $x_{c(2)} = 0.4$ (red point) either. In figure 6(b), we then consider as fixed observation location $x_{c(2)} = 0.8$ where among the poorest performances were obtained. As soon as a supplementary observation is considered away from that position (for instance $x_{c(1)} \leqslant 0.7$), reconstruction results are enhanced and

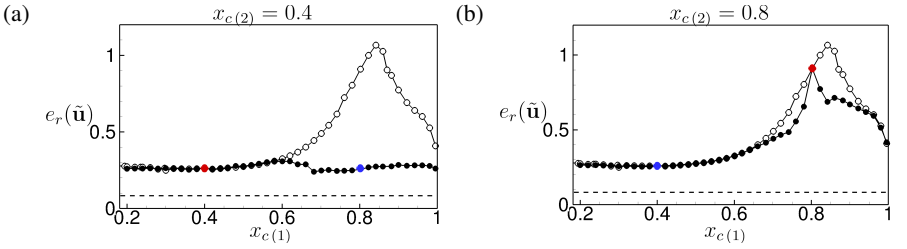

Figure 6: Reconstruction error $e_r(\tilde{\mathbf{u}})$ obtained with two C_p observations on the suction side (full circles). The location of the first observation $x_{c(1)}$ is varied while the second one $x_{c(2)}$ is fixed to (a) $x_{c(2)} = 0.4$ or (b) $x_{c(2)} = 0.8$ (red circles). Blue circles correspond to identical combinations of observations. Results obtained with single C_p observations are also reported with open circles for the sake of comparison.

α (°)	$e(\tilde{\mathbf{u}})$	$e_r(\tilde{\mathbf{u}})$	$e(\tilde{\mathbf{u}}_b)$	L_{rc}
8	0.024	0.436	0.055	0.04
10	0.025	0.283	0.088	0.14
11	0.030	0.264	0.114	0.22

Table 1: Absolute $e(\tilde{\mathbf{u}})$ and relative $e_r(\tilde{\mathbf{u}})$ reconstruction errors obtained with a single C_p observation at $x_c = 0.4$ on the suction side for various angles of attack. The absolute error $e(\tilde{\mathbf{u}}_b)$ for baseline RANS along with the chordwise extent L_{rc} of the recirculation region in the DNS results are also reported.

close to those obtained in successful single-data cases. This shows that using only two C_p observations instead of one significantly improves the robustness of the reconstruction as long as these two observations are not too close from each other. Incidentally, it was verified that relying on more observations is not worthwhile in the present configuration. As an example, the consideration of eight observations that are equally distributed on the suction side leads to $e_r(\tilde{\mathbf{u}}) = 0.238$, to be compared with the use of a single observation at $x_c = 0.4$ for which $e_r(\tilde{\mathbf{u}}) = 0.264$. Therefore, adding wall pressure observations is of interest for the robustness but not for the accuracy of the mean-flow reconstruction.

To conclude the investigation based on synthetic data from DNS, we reconstruct the mean flow for two other angles of attack, $\alpha = 8°$ and $10°$, again relying on a single observation of C_p at $x_c = 0.4$ on the suction side. The corresponding reconstruction errors are reported in table 1. It appears that data assimilation is successful in all considered cases. The absolute error $e(\tilde{\mathbf{u}})$, defined in (3.1), even slightly decreases when decreasing the angle of attack, indicating an even closer agreement with DNS at lower angles of attack. On the other hand, the relative error $e_r(\tilde{\mathbf{u}})$ (indicating an improvement compared to baseline RANS) increases for decreasing angles. This effect is attributed to reduced modelling errors in the baseline RANS prediction of attached turbulent boundary layers. Indeed, we observe that the absolute error $e(\tilde{\mathbf{u}}_b)$ of the baseline RANS solution decreases with the size L_{rc} of the recirculation region at the trailing edge, as reported in table 1. Still, for the case $\alpha = 8°$ where the turbulent boundary layer flow on the suction side of the airfoil is almost fully attached, the relative reconstruction error $e_r(\tilde{\mathbf{u}})$ is less than 0.5, indicating a significant enhancement in the flow estimation from single wall-pressure data even in this case.

Finally, we apply data assimilation to reconstruct the full mean flow at $\alpha = 11°$ using single

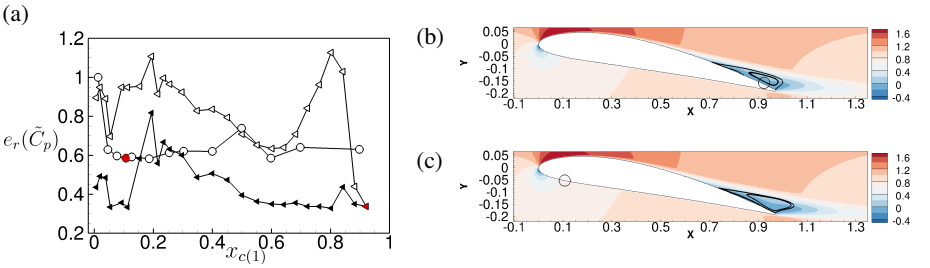

Figure 7: Experimental wall-pressure data assimilation for $\alpha = 11°$. (a) Error $e_r(\tilde{C}_p)$ when relying on a single pressure measurement at location $x_{c(1)}$ on the suction (open triangles) or pressure (open circles) side, or on two measurements on the suction side (filled triangles) where the location of the second measurement is kept fixed to $x_{c(2)} = 0.9$ (red triangle). (b,c) Reconstructed streamwise mean velocity with the single measurements at (b) $x_c = 0.9$ on the suction side and (c) $x_c = 0.1$ on the pressure side (red symbols in a).

or pairs of wall-pressure data from experiments. In this case where only N_m wall-pressure measurements are available (triangles in figure 1a), we assess the quality of the reconstruction by introducing a similar metric to (3.1) but based on all the available experimental wall-pressure measurements according to

$$e_r(\tilde{C}_p) = \frac{e(\tilde{C}_p)}{e(\tilde{C}_{p,b})}, \quad e(\tilde{C}_p) = \sqrt{\sum_{k=1}^{N_m} \frac{(\bar{C}_{p,e}(\boldsymbol{x}_k) - \tilde{C}_p(\boldsymbol{x}_k))^2}{\bar{C}_{p,e}(\boldsymbol{x}_k)^2}}, \tag{3.2}$$

where $\tilde{C}_p$ is the pressure coefficient of the reconstructed solution, while $\bar{C}_{p,e}$ and $\tilde{C}_{p,b}$ denote the experimental and baseline RANS wall-pressure coefficients, respectively. The position of the k-th sensor is denoted by $\boldsymbol{x}_k$. The error $e_r(\tilde{C}_p)$ is reported in figure 7(a) for various reconstructions, and we first consider results that are obtained with a single pressure measurement on the pressure (open circles) or suction (open triangles) side. For most measurements on the pressure side, appreciable improvement over the whole C_p distribution compared to baseline RANS is achieved. Results appear more contrasted for measurements at the suction side. Locations for which $e_r(\tilde{C}_p)$ remains close to 1 seem to well coincide with measurement values that are close to RANS ones, as around $x_c = 0.2$ and $x_c = 0.8$ (see figure 1a). Similarly as in the synthetic case, it appears that relying on pairs of measurements on the suction side significantly enhances the robustness of the reconstruction results (filled triangles). Selecting the measurement locations for which the minimum value of $e_r(\tilde{C}_p)$ is reached at the suction and pressure sides respectively in the single-data case, the corresponding reconstructed mean-velocity fields are illustrated in figures 7(b,c). The latter remarkably exhibit a recirculation region at the trailing edge that is similar to that in the DNS results. Although one should be here cautious in relying on such a metric as the experimental and DNS flows are likely to differ, it is still interesting to note that the relative error with respect to the DNS mean-velocity field verifies $e_r(\tilde{\mathbf{u}}) < 0.37$ for these reconstructions, which is comparable to values obtained with DNS C_p data. We may finally stress that considering a three-dimensional numerical model could here further enhance the reconstruction results since the experimental mean flow is likely three-dimensional, unlike that from DNS.

4. Conclusion

A variational data assimilation approach has been employed to reconstruct the full turbulent mean flow around a NACA4412 profile based on RANS modelling and extremely limited

wall data that are extracted from DNS or experiments. Remarkably, this approach has been demonstrated to dramatically improve baseline RANS results relying on observation of wall pressure at a single location on the airfoil. Despite the seemingly under-determined character of such a reconstruction problem, data assimilation has been able to accurately recover the full mean flow and the initially mispredicted strong separation and recirculation phenomena at the trailing edge in particular. This finding has appeared quite robust with respect to the observation location for both DNS and experimental data. Such reconstruction results could not be achieved when considering skin-friction observations. The present findings are therefore particularly encouraging concerning the potentialities of data assimilation in flow reconstruction for complex aerodynamic applications. On the experimental side, the present results suggest that the realization of a few pressure measurements is more effective than heavily instrumenting the studied airfoils. On the numerical and modelling sides, the need of reference data for machine-learning techniques as considered to obtain data-driven predictive turbulence models (Duraisamy 2021) seems alleviated if extremely scarce wall-pressure information is sufficient to satisfactorily calibrate RANS models.

Acknowledgements. The authors are grateful to M. Costes, V. Gleize, I. Mary and F. Richez for the generation and processing of the DNS results. The authors also thank F. Bouvier and V. Brion for producing the experimental data.

Declaration of interests. The authors report no conflict of interest.

REFERENCES

Belligoli, Z., Dwight, R. & Eitelberg, G. 2019 Assessment of a Data Assimilation Technique for Wind Tunnel Wall Interference Corrections. *AIAA Aviation 2019 Forum* p. 0939.

Ben Ali, M. Y., Tissot, G., Aguinaga, S., Heitz, D. & Mémin, E. 2022 Mean wind flow reconstruction of a high-rise building based on variational data assimilation using sparse pressure measurements. *Journal of Wind Engineering and Industrial Aerodynamics* **231**, 105204.

Buchta, D. A., Laurence, S. J. & Zaki, T. A. 2022 Assimilation of wall-pressure measurements in high-speed flow over a cone. *Journal of Fluid Mechanics* **947**, R2.

Cato, A. S., Volpiani, P. S., Mons, V., Marquet, O. & Sipp, D. 2023 Comparison of different data-assimilation approaches to augment RANS turbulence models pp. hal–04170127.

Duraisamy, K. 2021 Perspectives on machine learning-augmented Reynolds-averaged and large eddy simulation models of turbulence. *Physical Review Fluids* **6**, 050504.

Franceschini, L., Sipp, D. & Marquet, O. 2020 Mean-flow data assimilation based on minimal correction of turbulence models: Application to turbulent high reynolds number backward-facing step. *Physical Review Fluids* **5**, 094603.

Gleize, V., Costes, M. & Mary, I. 2022 Numerical simulation of NACA4412 airfoil in pre-stall conditions. *International Journal of Numerical Methods for Heat & Fluid Flow* **32**, 1375–1397.

Hecht, F. 2012 New development in FreeFem++. *Journal of Numerical Mathematics* **20**, 251–265.

Kato, H., Yoshizawa, A., Ueno, G. & Obayashi, S. 2015 A data assimilation methodology for reconstructing turbulent flows around aircraft. *Journal of Computational Physics* **283**, 559–581.

Li, S., He, C. & Liu, Y. 2022 A data assimilation model for wall pressure-driven mean flow reconstruction. *Physics of Fluids* **34**, 015101.

Mons, V. & Marquet, O. 2021 Linear and nonlinear sensor placement strategies for mean-flow reconstruction via data assimilation. *Journal of Fluid Mechanics* **923**, A1.

Singh, A. & Duraisamy, K. 2016 Using field inversion to quantify functional errors in turbulence closures. *Physics of Fluids* **28**, 045110.

Spalart, P. R. & Allmaras, S. R. 1994 A one-equation turbulence model for aerodynamic flows. *La Recherche Aérospatiale* **1**, 5–21.

Symon, S., Dovetta, N., McKeon, B. J., Sipp, D. & Schmid, P. J. 2017 Data assimilation of mean velocity from 2D PIV measurements of flow over an idealized airfoil. *Experiments in fluids* **58**, 1–17.

Xiao, H. & Cinnella, P. 2019 Quantification of model uncertainty in RANS simulations: A review. *Progress in Aerospace Sciences* **51**, 1–31.